

RePoseDM: Recurrent Pose Alignment and Gradient Guidance for Pose Guided Image Synthesis

Anant Khandelwal
Glance AI

anant.iitd.2085@gmail.com

Abstract

Pose-guided person image synthesis task requires re-rendering a reference image, which should have a photorealistic appearance and flawless pose transfer. Since person images are highly structured, existing approaches require dense connections for complex deformations and occlusions because these are generally handled through multi-level warping and masking in latent space. The feature maps generated by convolutional neural networks do not have equivariance, and hence multi-level warping is required to perform pose alignment. Inspired by the ability of the diffusion model to generate photorealistic images from the given conditional guidance, we propose recurrent pose alignment to provide pose-aligned texture features as conditional guidance. Due to the leakage of the source pose in conditional guidance, we propose gradient guidance from pose interaction fields, which output the distance from the valid pose manifold given a predicted pose as input. This helps in learning plausible pose transfer trajectories that result in photorealism and undistorted texture details. Extensive results on two large-scale benchmarks and a user study demonstrate the ability of our proposed approach to generate photorealistic pose transfer under challenging scenarios. Additionally, we demonstrate the efficiency of gradient guidance in pose-guided image generation on the HumanArt dataset with fine-tuned stable diffusion.

1. Introduction

Skeleton-guided image synthesis presents a formidable challenge within the domain of computer vision, offering a diverse array of applications spanning e-commerce, virtual reality, the metaverse, and the entertainment industries, aimed at content generation. Furthermore, these algorithms hold promise in enhancing performance via data augmentation for downstream tasks such as person re-identification [45]. The main challenge here is to generate photorealistic images that adhere to the specified target pose and appearance derived from the source image. In the literature, a

variety of techniques have been introduced, such as generative adversarial networks (GANs), diffusion models (DM), and variational autoencoders (VAE). Generally, all of them used CNNs (convolutional neural networks), which suffer from the problem of spatial transformation [35] and generation of equivariant feature maps [4]. To address the issue of spatial feature transformation, stacked CNNs have been introduced to expand the receptive field from local to global. However, transitioning from local to global can lead to the loss of fine-grained details in the source appearance. Flow-based networks [20, 27, 32] handle efficient spatial transformations, but they exhibit diminished performance in scenarios involving complex deformations and severe occlusions [28]. Since human images are highly structured, addressing complex deformations and occlusions necessitates multi-level warping and masking in latent space. However, this stacked warping approach was still unable to fully resolve the issue, as it tended to diminish the fine-grained details of the source appearance [3, 6]. GAN or VAE methods, whether flow-based or stacked CNNs, encounter challenges related to appearance deformations such as blurry details or low-quality outputs. Conversely, diffusion-based models rely on the iterative reduction of noise, modeled through CNN and attention mechanisms. Attention mechanisms, as described by Vaswani et al. [35], possess the capability of capturing dependencies by directly computing the interactions between any two positions. Therefore, diffusion models should theoretically be able to achieve perfect alignment of the source image and target pose through cross-attention. Unfortunately, in practice, due to the lack of equivariance between feature maps obtained from CNNs, the interaction positions cannot be decoded well by the attention mechanism. Hence, to address this issue, we proposed *Recurrent Pose Alignment* to repeatedly align the source image with a given target pose (shown in Supp. Figure 8). Injecting these pose-aligned features into the cross-attention in U-Net reduce the pose alignment error. It is based on multi-level warping, but it fails in cases of severe occlusions. Therefore, we propose *gradient-guided* training/sampling from diffusion models to further reduce the pose error in a lo-

calized manner. Our major contributions are as follows:

- We proposed a method called *Recurrent Pose Alignment* as a conditional block within the error prediction module in the diffusion model, aiming to reduce the leakage of the source pose into the denoising pipeline. Additionally, we establish the practical groundwork for multi-level warping, necessary for addressing equivariance in CNN feature maps.
- We proposed a novel *Gradient Guidance* technique to enforce the poses generated through interactions with source appearances to adhere to valid pose manifolds.
- We demonstrated improvements in both pose correction and the accurate generation of source appearance in pose-guided person image synthesis on the DeepFashion, HumanArt, and Market-1501 datasets.

2. Related Work

With the significant success of diffusion-based models for conditional image synthesis [15], an attempt known as PIDM [2] has been proposed for photorealistic image synthesis given the target pose and source image. PIDM [2] proposed to denoise the noise concatenated with the target pose image, conditioned on the source image. This process aims to inject the source appearance features into the cross-attention of U-Net. However, the feature map produced by CNNs lacks equivariance, causing the attention mechanism to struggle in accurately mapping source features to the target pose. Additionally, some GAN-based methods [10] simply concatenate the source pose, target image, and target pose as input to obtain the target image, leading to feature misalignment. To address this issue, the method proposed in [11] suggests disentangling the guidance from pose and source appearance using skip-connections in U-Net. Another method proposed in [32] introduces deformable skip connections for efficient spatial transformation. This approach breaks down the overall transformation into a series of local affine transformations, thereby addressing the issue of equivariance in CNN feature maps. Flow-based methods [18, 20, 27] are based on the idea of warping the source appearance with the target pose. GFLA [27] proposes global flow fields and an occlusion mask for mapping the source image to the target pose. ADGAN [25] utilizes a texture encoder to extract appearance features for different body parts and feeds them into residual AdaIN blocks to synthesize the target image. PISE [39], SPGnet [24], and CASD [44] all employ parsing maps with variations in encoder and decoder to generate the final image. CoCosNet [43] uses an attention mechanism to extract appearance features between cross-domain images. NTED [29], a method based on distribution operation, proposes obtaining semantically similar texture features by aligning the semantic textures of the source image with the semantic filters for the target pose. All the aforementioned approaches propose a

method to map the source to the target pose in some way but do not involve pose correction. We proposed *gradient guidance* to iteratively correct the pose.

3. Proposed Method

Overall Framework: Fig.1 displays the overall architecture of our proposed generative model, *RePoseDM*. Given a source image I_S and a target pose P , our goal is to generate a target image that strictly follows the target pose and has the same appearance as the source. This is achieved using the conditional guidance into U-Net from pose-aligned texture features (*Recurrent Pose Alignment*) and gradient guidance (from *Pose Interaction Fields*) to learn the plausible trajectories for the target pose generation. We will discuss next (Section 3.1) the training of conditional diffusion models with gradient guidance, followed by *Recurrent Pose Alignment* in Section 3.2 and *Pose Interaction Fields* in Sec.3.3.

3.1. Appearance Conditioned Diffusion Model

RePoseDM is based on the generative scheme of iterative noise reduction as proposed in Denoising diffusion probabilistic model (DDPM) [15]. The general idea behind DDPM is the combination of two processes: *forward* diffusion and *backward* denoising. During the forward (diffusion) process, it gradually adds noise to the data sampled from the target distribution $\mathbf{y}_0 \sim q(\mathbf{y}_0)$, and the backward (denoising) process aims to eliminate this noise. The forward process is described by the Markov chain with the following distribution:

$$q(\mathbf{y}_T|\mathbf{y}_0) = \prod_{t=1}^T q(\mathbf{y}_t|\mathbf{y}_{t-1}), \text{ where} \\ q(\mathbf{y}_t|\mathbf{y}_{t-1}) = \mathcal{N}(\mathbf{y}_t; \sqrt{1 - \beta_t}\mathbf{y}_{t-1}, \beta_t\mathbf{I}). \quad (1)$$

Here, the noise schedule β_t is an increasing sequence of $t \in [0, T]$ with $\beta_t \in (0, 1)$. Using the notations $\bar{\alpha}_t = \prod_{s=1}^t \alpha_s$, $\alpha_t = 1 - \beta_t$. we can sample from $q(\mathbf{y}_t|\mathbf{y}_0)$ in a closed form at an arbitrary time step t : $\mathbf{y}_t = \sqrt{\bar{\alpha}_t}\mathbf{y}_0 + \sqrt{1 - \bar{\alpha}_t}\epsilon$, where $\epsilon \in \mathcal{N}(0, \mathbf{I})$. For the denoising process, we predict the noise $\epsilon_\theta(\mathbf{y}_t, t, \mathbf{P}, \mathbf{I}_S)$ using the neural network (U-Net) using which we can predict the next-step sample \mathbf{y}_{t-1} from the noisy sample \mathbf{y}_t at previous time-step given as:

$$\mathbf{y}_{t-1} = \frac{1}{\sqrt{\alpha_t}} \left(\mathbf{y}_t - \frac{1 - \alpha_t}{\sqrt{1 - \bar{\alpha}_t}} \epsilon_\theta(\mathbf{y}_t, t, \mathbf{P}, \mathbf{I}_S) \right) + \sigma_t \epsilon \quad (2)$$

where $\epsilon \sim \mathcal{N}(0, \mathbf{I})$, σ_t^2 is variance which is β in DDPM[15]. With this iterative process we sample the clean image \mathbf{y}_0 from the noise $\mathbf{y}_T \in \mathcal{N}(0, \mathbf{I})$.

Noise Prediction $\epsilon_\theta(\mathbf{y}_t, t, \mathbf{P}, \mathbf{I}_S)$: Given the target pose \mathbf{P}

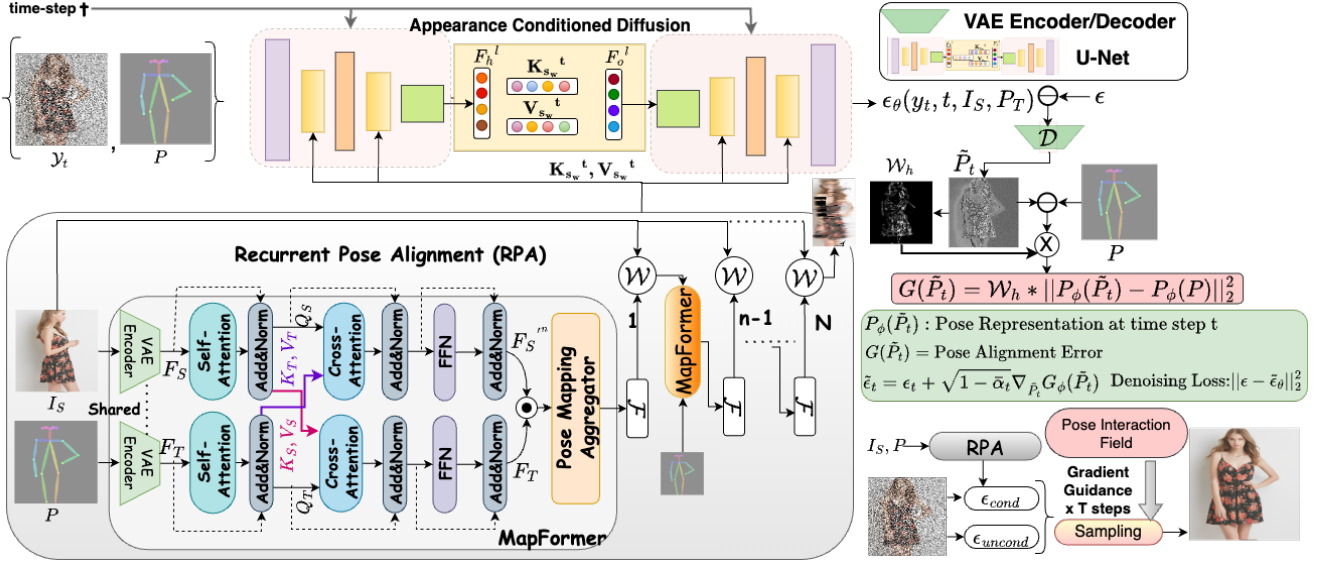


Figure 1. **RePoseDM**: Architecture of our proposed U-Net based Diffusion Model with *Recurrent Pose Alignment* and *Gradient Guidance* from *Pose Interaction Fields*. Warped source appearance features are fed to U-Net using cross-attention.

and noisy sample \mathbf{y}_t , we concatenate the representation of these two (obtained from VAE encoder) before passing it to the noise predictor network **U-Net**. The target pose \mathbf{P} will guide each intermediate denoising step to synthesize the final person image for the given pose and bind the garment texture on that pose using the warped texture features obtained from the *Recurrent Pose Alignment Block* (explained in Section 3.2). This block, recurrently at each step, warps the source image with the target pose \mathbf{P} to produce the texture features which can be superimposed onto the target pose in the denoising process. This ensures no source pose leakage and hence avoids any additional noise that can cause pose misalignment. However, as shown in Fig. 1, for the challenging transfer of poses i.e. left side pose (source) to the front pose (target), there are deformations in predicted $\tilde{\mathbf{P}}_t$ which is termed as *pose alignment noise*. Due to this additional pose alignment noise, we train the denoising process using gradient guidance from *Pose Interaction Fields* (explained in Section 3.3) $G(\tilde{\mathbf{P}}_t)$, where $\tilde{\mathbf{P}}_t$ is the pose obtained from the denoised image which is obtained after subtracting ground truth noise ϵ from noise predicted by U-Net i.e. ϵ_θ . Let $\tilde{\epsilon}_\theta$ be the updated predicted noise including the pose alignment noise, incorporating this in the denoising training loss as:

$$L_{mse} = \mathbb{E}_{t \sim [0, T], \mathbf{y}_0 \sim q(\mathbf{y}_0), \epsilon} \|\epsilon - \tilde{\epsilon}_\theta(\mathbf{y}_t, t, \mathbf{P}, I_S)\|^2 \quad (3)$$

where $\mathbf{y}_t \sim q(\mathbf{y}_t | \mathbf{y}_0)$ is the noisy sample from the forward process. For an effective learning strategy in fewer steps, an additional loss term L_{vib} is proposed in [26], to learn the noise variance Σ_θ of the posterior distribution $q(\mathbf{y}_{t-1} | \mathbf{y}_t) = p_\theta(\mathbf{y}_{t-1} | \mathbf{y}_t) = \mathcal{N}(\mathbf{y}_t; \mu_\theta(\mathbf{y}_t, t, \mathbf{P}, I_S), \Sigma_\theta(\mathbf{y}_t, t, \mathbf{P}, I_S))$.

Instead of directly deriving $\mu_\theta, \Sigma_\theta$ from the neural network, we predict only the noise ϵ_θ from which the mean and variance are calculated [26]. The updated loss is given as:

$$L_{total} = L_{mse} + L_{vib} \quad (4)$$

3.2. Recurrent Pose Alignment

MapFormer: Given the source image I_S and the target pose image \mathbf{P} , these are mapped to their respective latent representations using VAE encoder. These latent representations are then fed to two key components: Attention and Pose Mapping Aggregator. Attention in **MapFormer** consists of both Self-Attention and Cross-Attention blocks for I_S and \mathbf{P} respectively. Both blocks perform region-specific attention to introduce the effect of multi-level warping from global \rightarrow non-local region \rightarrow local region. This is inspired by [8, 9, 12, 21], where multi-level warping of the source image is performed to cope with warping deformations due to non-equivariant feature maps for both images. Specifically, for the coordinate point \mathbf{x} , the region $\mathcal{N}(\mathbf{x})$, query Q , key K , and value V , the self-attention (self(.)) and cross-attention (cross(.)) are given as follows:

$$\begin{aligned} \text{self}(\mathbf{x}) &= \text{softmax} \left(\frac{Q_i(\mathcal{N}(\mathbf{x}))^T K_i(\mathcal{N}(\mathbf{x}))}{\sqrt{D}} \right) V_i(\mathcal{N}(\mathbf{x})) \\ \text{cross}(\mathbf{x}) &= \text{softmax} \left(\frac{Q_i(\mathcal{N}(\mathbf{x}))^T K_j(\mathcal{N}(\mathbf{x}))}{\sqrt{D}} \right) V_j(\mathcal{N}(\mathbf{x})) \end{aligned} \quad (5)$$

where i and j refer to the indices of images, denoting the query from one and the key, value from another. D is the

depth of the convolution layer calculating the representation of the region $\mathcal{N}(x)$. Similar to previous works [31, 38], residual connection, layer normalization, and feed-forward layers have been used, as shown in Fig. 1. Only 1 layer of self-attention and cross-attention is used with different kernel sizes for a fixed depth D of the convolution layer.

Pose Mapping Aggregator: Pose aggregation is performed with different kernels to accumulate the interaction between the source image and the target pose from global to localized regions. After calculating the intra/inter correspondences between the source image and the target pose for a given region $\mathcal{N}(\mathbf{x})$, the correlation between localized regions is determined as:

$$\mathbf{C}(\mathbf{x}, \mathbf{r}) = \text{ReLU}(\mathbf{F}'_T(\mathbf{x})^T \mathbf{F}'_S(\mathbf{x} + \mathbf{r})) \|\mathbf{r}\|_\infty \leq R \quad (6)$$

where \mathbf{F}'_S^n is the feature at step n after FFN, residual connection and layer norm as shown in Fig. 1. It is obtained from the warped input feature \mathbf{F}_S^{n-1} at previous step $n - 1$ (equation 9). R controls the radius of each local region and hence produce the correlation feature of size $H \times W \times (2R + 1) \times (2R + 1)$. The architecture of pose aggregator is similar to the previous works [3, 4, 31], it consists of 2 convolution layers and 1 max-pooling layer, with convolution layer of same depth D used during attention. Correlation is similar to cross-attention[31] where the output is the mapping of source features to pose-aligned features. At iteration n , the output of pose aggregator for specific region is denoted as ΔF^n .

Recurrent Pose Alignment: For each region $\mathcal{N}(x)$, the MapFormer and Pose-Aggregator produce the correlation map of pose-specific features for global to local regions in an iterative manner for $n \in [1, N]$. We introduce a recurrent accumulator \mathcal{F} to combine these features for all regions, which can be used to perform warping recursively. This ensures the accurate estimation of warped source features (finally F_S^N fed to the U-Net's Cross-Attention as shown in Fig. 1), reducing pose misalignment to the minimum possible. The recurrent accumulation is defined as:

$$\mathcal{F}^{n+1} = \mathcal{F}^n \Delta F^{n+1}, \text{ where} \quad (7)$$

$$\Delta F^{n+1} = \mathcal{M}(F_T, F_S^n) \text{ and} \quad (8)$$

$$F_S^n = \text{Encoder}(\mathcal{W}(I_S; \mathcal{F}^n)) \quad (9)$$

where \mathcal{M} is MapFormer with Pose Aggregator. For $n = 0$, $\mathcal{F}^0 = \Delta F^0 = \mathcal{M}(F_T, F_S)$, where $F_S = \text{Encoder}(I_S)$, Encoder is obtained from VAE encoder as discussed above.

3.3. Pose Interaction Fields

The warped image generated by recurrent pose alignment still has pose misalignment (as shown in Figure 1), which gets injected into U-Net at every time step t . Hence, the predicted noise $\epsilon_\theta(\mathbf{y}_t, t, P, I_S)$ contains this pose alignment

noise, which needs to be explicitly addressed in the loss function during the training of the denoising process. To alleviate this issue, we propose to guide the diffusion model with the distance between interaction poses generated from the diffusion model (shown by \tilde{P}_t in Fig. 1) and the valid pose. To calculate the distance, we obtain the pose representation from a pre-trained pose estimator model, i.e., HigherHRNet [7]. Inspired by *HumanSD* [17], we obtain the generated pose map \tilde{P}_t by applying the VAE decoder over the subtraction of noise predicted by U-Net from the ground truth noise, given as:

$$\tilde{P}_t = \text{VAE}_{\text{decoder}}(\epsilon - \epsilon_\theta(\mathbf{y}_t, t, P, I_S)) \quad (10)$$

We then use bottom-up pose estimator HigherHRNet [7] (pre-trained on MSCOCO [19] and Human-Art[16]) to get pose representation. Using pretrained model, we are able to localize the locations of human joints from the pose map generated by the diffusion model using the heatmap generated $H \in R^{H \times W \times k}$ where k is the number of joints. Summing and thresholding (threshold= 0.1) the heat maps across the joints give the heat map mask H_M which served as the weight W_h indicating exactly where the focus is required to reduce the pose alignment noise. Finally, we pass the pose \tilde{P}_t to the backbone of pose estimator to get the latent representation for the pose generated by the diffusion model and the valid pose. The pose alignment error is then calculated as:

$$G_\phi(\tilde{P}_t) = W_h * \|P_\phi(\tilde{P}_t) - P_\phi(P)\|_2^2 \quad (11)$$

Where P_ϕ represents the backbone of the pose estimator model, which provides the latent representation of the given pose. We multiply it with the weight W_h to get the error only at those locations where the pose is generated by the diffusion model. Inspired by recent work on neural distance fields to learn valid human pose manifolds [34] and robotic grasping manifolds [37], which provide information about how far an arbitrary pose is from a valid pose, in our case, the offset vector G_ϕ takes in the pose generated by the diffusion model and outputs how far it is from the target pose P . This offset vector $\Delta P = G_\phi(\tilde{P}_t)$ can generate the manifold of valid interaction poses for the pose generated by the diffusion model at step t : $\tilde{P}_t + \Delta P$. To ensure that the sample update from $\mathbf{y}_t \rightarrow \mathbf{y}_{t-1}$ lies on the correct pose manifold, we leverage gradient guidance as follows:

$$\mathbf{y}'_{t-1} = \mathbf{y}_{t-1} - \underbrace{\nabla_{\tilde{P}_t} G_\phi(\tilde{P}_t)}_{\Delta y_{0,t}} \quad (12)$$

where the next step sample \mathbf{y}_{t-1} is generated using equation 2. Specifically, if we add $\Delta y_{0,t}$ from equation 19 in equation 2, then following [1] the original forward equation $\mathbf{y}_t = \sqrt{\bar{\alpha}_t} \mathbf{y}_0 + \sqrt{1 - \bar{\alpha}_t} \epsilon$ is converted to:

$$\mathbf{y}_t = \sqrt{\bar{\alpha}_t}(\hat{\mathbf{y}}_{0,t} + \Delta y_{0,t}) + \sqrt{1 - \bar{\alpha}_t} \tilde{\epsilon}_t \quad (13)$$

where $\hat{y}_{0,t}$ is the estimated cleaned image using Tweedie’s formula[33], perturbed diffusion model given as:

$$\tilde{\epsilon}_t = \epsilon_t - \sqrt{\bar{\alpha}_t/(1 - \bar{\alpha}_t)}\Delta y_{0,t}, \quad (14)$$

where $\Delta y_{0,t} = -\eta \nabla_{\tilde{P}_t} G_\phi(\tilde{P}_t)$ for some scale factor η , leading to

$$\tilde{\epsilon}_t = \epsilon_t + \sqrt{1 - \bar{\alpha}_t} \nabla_{\tilde{P}_t} G_\phi(\tilde{P}_t) \quad (15)$$

suggesting the pose guided diffusion model. The previous work [1] sets the scale factor to $\eta = \sqrt{1 - \bar{\alpha}_t}$.

3.4. Sampling and Gradient Guidance

At test time, the samples are generated from the model with the input random noise $\mathbf{y}_T = \mathcal{N}(0, \mathbf{I})$ concatenated with the target pose P and the interaction conditioning F_S^N , which contains features of the source garment when interacted with the target pose P . The distribution $p(y_{t-1}|y_t, P, I_S)$ governs the sampling process from $t = T$ to $t = 0$ in iterative manner. Following, the previous works [14] we also leveraged the classifier-free guidance. This implies that we have conditional and unconditional sample from the model and combine them as follows

$$\epsilon_{cond} = \epsilon_{uncond} + w_c * (\epsilon_{interaction} + \sqrt{1 - \bar{\alpha}_t} \epsilon_{gradient}) \quad (16)$$

where the strength of interaction conditioning is controlled by scalar w_c , the unconditioned prediction is given as $\epsilon_{uncond} = \epsilon_\theta(\mathbf{y}_t, t, \emptyset, \emptyset)$ where the condition of target pose P , and source image I_S has been set to null, which implies there is no interaction conditioning F_S^N , on the other hand the conditioned prediction is $\epsilon_\theta(\mathbf{y}_t, t, P, I_S)$, where the interaction features F_S^N are given as input to cross-attention of U-Net. Additionally, we leveraged gradient guidance for the pre-trained pose estimation model, to account for pose alignment error during denoising process, this is given as $\epsilon_{gradient} = \nabla_{\tilde{P}_t} G_\phi(\tilde{P}_t)$, which is combined as in eqn 15. During training, the diffusion model learns both conditioned and unconditioned distributions by randomly setting $P, I_S = \emptyset$ for $p\%$ of examples, which learns the distribution $p(\mathbf{y}_0)$ faithfully and leverage it during inference.

4. Experiments

Datasets: Experiments were carried out on the In-Shop Clothes Retrieval Benchmark of DeepFashion [22] and the Market-1501 [42] datasets. The DeepFashion dataset contains 52,712 high-resolution images of men and women fashion models, while the Market-1501 dataset contains 32,668 low-resolution images. Pose skeletons were extracted using OpenPose [5]. For DeepFashion, following the dataset splits in [45], there are a total of 101,966 pairs

Dataset	Methods	FID(↓)	SSIM(↑)	LPIPS(↓)
DeepFashion (256 × 176)	Def-GAN	18.457	0.6786	0.2330
	PATN	20.751	0.6709	0.2562
	ADGAN	14.458	0.6721	0.2283
	PISE	13.610	0.6629	0.2059
	GFLA	10.573	0.7074	0.2341
	DPTN	11.387	0.7112	0.1931
	CASD	11.373	0.7248	0.1936
	NTED	8.6838	0.7182	0.1752
	PIDM	6.3671	0.7312	0.1678
	RePoseDM (Ours)	5.1986	0.7923	0.1463
DeepFashion (512 × 352)	CocosNet2	13.325	0.7236	0.2265
	NTED	7.7821	0.7376	0.1980
	PIDM	5.8365	0.7419	0.1768
	RePoseDM (Ours)	4.7284	0.7944	0.1566
Market-1501 (128 × 64)	Def-GAN	25.364	0.2683	0.2994
	PTN	22.657	0.2821	0.3196
	GFLA	19.751	0.2883	0.2817
	DPTN	18.995	0.2854	0.2711
	PIDM	14.451	0.3054	0.2415
	RePoseDM (Ours)	13.689	0.3284	0.2206

Table 1. Quantitative Comparision of **RePoseDM** with SOTA methods in terms of FID, SSIM, LPIPS

in the training set and 8,570 pairs in the testing set. For both datasets, the training and test sets do not contain overlapping person identities. The images from both datasets vary in factors such as illumination, background, and view-point angles. Evaluation metrics are explained in App. 7 and implementation details are given in App. 8.

4.1. Quantitative and Qualitative Comparisons

We compared our model *RePoseDM* both qualitatively (Fig.2, 3) and quantitatively (Tab.1) with several state-of-the-art methods, namely, PIDM [2], NTED [29], CocosNet2 [43], CASD [44], DPTN [40], Def-GAN [32], PATN [45], ADGAN [25], PISE [39], and GFLA [27]. For qualitative comparison, we experimented with the DeepFashion dataset at multiple resolutions, i.e., 256 × 176 and 512 × 352 images. For Market-1501, we used 128 × 64 images. Tab.1 shows that our model achieved the best results in all three metrics: FID, SSIM, and LPIPS, indicating superior photorealism in the generated images (Fig.2), while preserving finer details like texture and cloth warping for the given target pose. Moreover, the improvement over SSIM and LPIPS demonstrates better structural properties, not only in terms of generating the target pose but also in accurate garment reconstruction for a given target pose. Fig.2 presents a qualitative visual comparison of our method with state-of-the-art frameworks on the DeepFashion dataset. The synthesized images from other methods were obtained using the pre-trained models provided by the corresponding authors. From the results, it can be observed that ADGAN [25] and PISE [39] consistently perform poorly in terms of the quality of generated images and cannot retain shape and texture



Figure 2. Qualitative comparison of several SOTA methods on the DeepFashion dataset. The inputs shown are target pose and source image, ground truth shows the image in target pose. Images generated from several methods are shown next. **Ours** indicate RePoseDM



Figure 3. Qualitative comparison from several SOTA methods are shown on Market-1501 dataset. **Ours** indicate RePoseDM

details. GFLA [27] improves on the texture details (4th and 8th row left columns, and 8th row right column) but still struggles to generate reasonable results in unseen regions of images (6th row left column, and 2nd and 4th row right columns). CASD [44] and NTED [29] show slight improvements compared to methods before them but still struggle to preserve the source appearance in complex scenarios (9th and 1st rows in left column, and 3rd, 5th, and 10th rows in right column). Although PIDM [2] generates sharp images,

it either has problems with incorrect pose (5th and 7th row right columns, 5th row left column) or missing texture (2nd, 4th, 6th, 9th, and 10th row left columns, and 2nd, 3rd, 6th, 8th, and 10th row right columns). Our method minimizes texture errors and faithfully generates images for invisible regions as well. With pose guidance, our method generates the correct pose in those places where PIDM [2] missed, as shown in Fig.2 (5th and 7th row right columns, 5th row left column). Additionally, we provide qualitative results on the Market-1501 dataset as shown in Fig.3. The Market-1501 dataset contains challenging backgrounds, and as shown in Fig.3, our method is still able to generate photorealistic images while faithfully retaining the source appearance in the target pose. Additionally, some results on appearance control are shown in Fig.4, where given the reference image needs to be transformed to wearing a garment provided in the garment image. We chose challenging poses of garment images and demonstrated that our method faithfully generates those invisible regions in a reference image.

4.2. Human Perception Study

To validate the effectiveness of our method in terms of human perception, the results are evaluated by 100 participants in two schemes: 1) For comparison with ground truth



Figure 4. Editing Capability of RePoseDM by controlling garment appearance of target image using source image.

Methods	FID(↓)	SSIM(↑)	LPIPS(↓)
B1	7.5274	0.7189	0.1912
B2	6.9113	0.7055	0.1634
RePoseDM	5.1986	0.7923	0.1463

Table 2. Ablation Studies showing the impact made *Recurrent Pose Alignment* and *Gradient Guidance*

images, we randomly selected 30 images from the test set and 20 images generated by our method. Participants are required to mark the image generated by our method or from ground truth image. Following [2, 44, 45], we adopted two metrics, namely, *R2G* and *G2R*. *R2G* is the percentage of real images classified as generated images, and *G2R* is the percentage of generated images classified as real images. 2) For comparison with other methods, we randomly selected 30 images from the test set and finally presented 30 such sets containing the source image, target pose, image generated by our method, and baselines. Following [2], we quantified this in terms of a metric named *JAB*, which represents the percentage of images from our method that are considered best among all other methods. For each of the three metrics, higher values indicate better performance of our method. Results presented in Fig.7 demonstrate that *RePoseDM* outperforms all other methods. For instance, *RePoseDM* achieves *G2R* = 62%, which is nearly 15% better than the second-best model, and the *JAB* metric is 82%, favoring images generated by our method over others.



Figure 5. Qualitative comparison with ablation baselines B1 & B2

Models	Image Quality FID↓	Pose Accuracy			
		AP↑	AP(m)↑	CAP↑	PCE↓
HumanSD	26.28	31.85	24.95	59.11	1.61
RePoseSD	24.83	33.79	26.85	61.25	1.56

Table 3. Quantitative comparison b/w HumanSD and RePoseSD

4.3. Ablation Study

We conducted detailed ablation studies to demonstrate the merits of contributions made towards pose-guided person image synthesis. Tab.2 shows the quantitative results on the DeepFashion dataset, comparing *RePoseDM* with several ablation baselines to quantify the contributions made by *Recurrent Pose Alignment* and *Gradient Guidance*. The baseline B1 is the baseline without *Gradient Guidance* and *Recurrent Pose Alignment*. Specifically, it consists of a conditioned U-Net-based noise prediction module where noise and the target pose are concatenated as input, and the source image is passed through a simple CNN encoder to provide texture conditioning to the U-Net. Baseline B1 is PIDM only. Baseline B2 incorporates pose alignment conditions into the U-Net model from the *Recurrent Pose Alignment* block but without any gradient guidance. Finally, REPOSEDM is compared with two baselines, B1 and B2, as shown in Tab.2 and Fig.5. Qualitatively, as shown in Fig.5, baseline B1 generates images with incorrect pose and texture, while baseline B2 generates images lacking in pose quality.

4.4. Effectiveness of Gradient Guidance

We further applied and tested the proposed *Gradient Guidance* in the pre-trained text-based diffusion model, Stable Diffusion v2-1 (SD) [30]. We fine-tuned the SD model on 0.2M text-image-pose pairs obtained from the LAION-Human dataset [17] and tested it on the validation set of the Human-Art dataset [16]. Specifically, we concatenated the noise and pose representation obtained from the VAE encoder and input these to the text-conditioned U-Net for noise prediction at each step of the denoising process. During training, we modified ϵ_t to $\tilde{\epsilon}_t$ according to Equation 15 containing gradient guidance for predicted pose represen-



Figure 6. Qualitative comparison b/w HumanSD and RePoseSD. HumanSD and RePoseSD trained on 0.2M text-image-pose pairs randomly sampled from *LAION-Human*

tation obtained from the pre-trained pose estimator High-erHRNet [7]. The pose-guided training loss for stable diffusion is given as:

$$L_{LDM} = E_{t,z,\epsilon} [\|\epsilon - \tilde{\epsilon}_\theta(\sqrt{\bar{\alpha}_t}z_0 + \sqrt{1 - \bar{\alpha}_t}\epsilon, c, t)\|_2^2] \quad (17)$$

where z_0 is the latent embedding of a sample x_0 , c is the text (prompt) embedding, $\bar{\alpha}_t$, ϵ_θ and ϵ is the same as that in vanilla diffusion models. Fig.6 presents the qualitative comparison of pose-guided image generation obtained from *HumanSD* (shown in the middle after the target pose) and *REPOSESD* (shown on the right after the image from *HumanSD*). We name our model *REPOSESD*, which is obtained after fine-tuning with our proposed gradient guidance on the SD model. Clearly, the images generated by our method show better pose alignment, especially in cases where the target pose comprises multiple poses. For example, consider the case of *Jesus*: our method is able to generate the correct pose of the hands and legs of the other two persons. Similarly, in other cases like *dance*, where the hand should be close to the head, and *football*, where the boys should have opposite poses, our method accurately captures these details. Tab.3 shows the quantitative comparison of our method with *HumanSD* [17], which is the current state-of-the-art in text-based pose-guided generation. Our method outperforms in terms of all three metrics: image quality, pose accuracy, and Text Consistency, using the same metrics as used in [16].

4.5. Person Re-Identification

We evaluate the applicability of images generated from *RePoseDM* in improving the performance of the downstream task of person re-identification (re-ID) with data augmentation using images generated from our method. We perform this evaluation with data augmentation on the Market-1501 dataset. Specifically, we randomly sample 20%, 40%, 60%, and 80% from the training dataset and augment each set with images generated from our method for the ran-

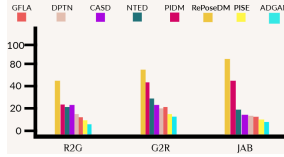


Figure 7. Human Perception Study on DeepFashion dataset showing R2G, G2R and JAB metrics. RePoseDM outperforms other methods.

Models	Real Images(%)			
	20%	40%	60%	80%
PTN	54.9	56.7	66.5	71.9
GFLA	58.1	60.1	68.2	73.4
DPTN	58.1	62.6	69.0	74.2
PIDM	61.5	64.9	71.8	75.7
RePoseDM	63.6	65.5	72.4	76.1

Table 4. Person re-ID results showing mAP scores of ResNet50 trained on augmented with images generated from several methods

domly selected source image and randomly selected target pose. To facilitate the comparison of our method with other baselines, we repeat the above procedure for augmented set creation from images generated with other baselines as well. Specifically, we select PIDM [2], PTN [45], GFLA [27], and DPTN [40]. Tab.4 presents the results using the ResNet50 backbone on each of the individual sets with data augmentation from different methods. The performance of the fine-tuned ResNet50 on data augmented with our method outperforms all the other methods.

5. Conclusion

In conclusion, we present a novel approach for pose-guided person image synthesis, leveraging recurrent pose alignment and gradient guidance from pose interaction fields. By providing pose-aligned texture features as conditional guidance, our method achieves photorealistic results with flawless pose transfer, even in challenging scenarios. Extensive experiments on large-scale benchmarks and a user study demonstrate the effectiveness of our approach in generating high-quality images. Furthermore, our method showcases efficiency and stability in generating pose-guided images, as demonstrated on the HumanArt dataset with fine-tuned stable diffusion. Overall, our approach advances the state-of-the-art in pose-guided image synthesis, offering applications in various fields such as virtual try-on, digital entertainment, and augmented reality.

References

- [1] Arpit Bansal, Hong-Min Chu, Avi Schwarzschild, Soumyadip Sengupta, Micah Goldblum, Jonas Geiping, and Tom Goldstein. Universal guidance for diffusion models. In *Proceedings of the IEEE/CVF Conference on Computer Vision and Pattern Recognition*, pages 843–852, 2023. 4, 5
- [2] Ankan Kumar Bhunia, Salman Khan, Hisham Cholakkal, Rao Muhammad Anwer, Jorma Laaksonen, Mubarak Shah, and Fahad Shahbaz Khan. Person image synthesis via denoising diffusion model. In *Proceedings of the IEEE/CVF Conference on Computer Vision and Pattern Recognition*, pages 5968–5976, 2023. 2, 5, 6, 7, 8
- [3] Si-Yuan Cao, Jianxin Hu, Zehua Sheng, and Hui-Liang Shen. Iterative deep homography estimation. In *Proceedings of the IEEE/CVF Conference on Computer Vision and Pattern Recognition*, pages 1879–1888, 2022. 1, 4
- [4] Si-Yuan Cao, Runmin Zhang, Lun Luo, Beinan Yu, Zehua Sheng, Junwei Li, and Hui-Liang Shen. Recurrent homography estimation using homography-guided image warping and focus transformer. In *Proceedings of the IEEE/CVF Conference on Computer Vision and Pattern Recognition*, pages 9833–9842, 2023. 1, 4
- [5] Zhe Cao, Tomas Simon, Shih-En Wei, and Yaser Sheikh. Realtime multi-person 2d pose estimation using part affinity fields. In *Proceedings of the IEEE conference on computer vision and pattern recognition*, pages 7291–7299, 2017. 5
- [6] Che-Han Chang, Chun-Nan Chou, and Edward Y Chang. Clkn: Cascaded lucas-kanade networks for image alignment. In *Proceedings of the IEEE conference on computer vision and pattern recognition*, pages 2213–2221, 2017. 1
- [7] Bowen Cheng, Bin Xiao, Jingdong Wang, Honghui Shi, Thomas S Huang, and Lei Zhang. Higherhrnet: Scale-aware representation learning for bottom-up human pose estimation. In *Proceedings of the IEEE/CVF conference on computer vision and pattern recognition*, pages 5386–5395, 2020. 4, 8
- [8] Taco Cohen and Max Welling. Group equivariant convolutional networks. In *International conference on machine learning*, pages 2990–2999. PMLR, 2016. 3
- [9] Taco S Cohen, Mario Geiger, Jonas Köhler, and Max Welling. Spherical cnns. *arXiv preprint arXiv:1801.10130*, 2018. 3
- [10] Antonia Creswell, Tom White, Vincent Dumoulin, Kai Arulkumaran, Biswa Sengupta, and Anil A Bharath. Generative adversarial networks: An overview. *IEEE signal processing magazine*, 35(1):53–65, 2018. 2
- [11] Patrick Esser, Ekaterina Sutter, and Björn Ommer. A variational u-net for conditional appearance and shape generation. In *Proceedings of the IEEE conference on computer vision and pattern recognition*, pages 8857–8866, 2018. 2
- [12] Joao F Henriques and Andrea Vedaldi. Warped convolutions: Efficient invariance to spatial transformations. In *International Conference on Machine Learning*, pages 1461–1469. PMLR, 2017. 3
- [13] Martin Heusel, Hubert Ramsauer, Thomas Unterthiner, Bernhard Nessler, and Sepp Hochreiter. Gans trained by a two time-scale update rule converge to a local nash equilibrium. *Advances in neural information processing systems*, 30, 2017. 1
- [14] Jonathan Ho and Tim Salimans. Classifier-free diffusion guidance. *arXiv preprint arXiv:2207.12598*, 2022. 5
- [15] Jonathan Ho, Ajay Jain, and Pieter Abbeel. Denoising diffusion probabilistic models. *Advances in neural information processing systems*, 33:6840–6851, 2020. 2
- [16] Xuan Ju, Ailing Zeng, Jianan Wang, Qiang Xu, and Lei Zhang. Human-art: A versatile human-centric dataset bridging natural and artificial scenes. In *Proceedings of the IEEE/CVF Conference on Computer Vision and Pattern Recognition*, pages 618–629, 2023. 4, 7, 8
- [17] Xuan Ju, Ailing Zeng, Chenchen Zhao, Jianan Wang, Lei Zhang, and Qiang Xu. Humansd: A native skeleton-guided diffusion model for human image generation. *arXiv preprint arXiv:2304.04269*, 2023. 4, 7, 8
- [18] Yining Li, Chen Huang, and Chen Change Loy. Dense intrinsic appearance flow for human pose transfer. In *Proceedings of the IEEE/CVF Conference on Computer Vision and Pattern Recognition*, pages 3693–3702, 2019. 2
- [19] Tsung-Yi Lin, Michael Maire, Serge Belongie, James Hays, Pietro Perona, Deva Ramanan, Piotr Dollár, and C Lawrence Zitnick. Microsoft coco: Common objects in context. In *Computer Vision—ECCV 2014: 13th European Conference, Zurich, Switzerland, September 6–12, 2014, Proceedings, Part V 13*, pages 740–755. Springer, 2014. 4
- [20] Wen Liu, Zhixin Piao, Jie Min, Wenhan Luo, Lin Ma, and Shenghua Gao. Liquid warping gan: A unified framework for human motion imitation, appearance transfer and novel view synthesis. In *Proceedings of the IEEE/CVF International Conference on Computer Vision*, pages 5904–5913, 2019. 1, 2
- [21] Yuan Liu, Zehong Shen, Zhixuan Lin, Sida Peng, Hujun Bao, and Xiaowei Zhou. Gift: Learning transformation-invariant dense visual descriptors via group cnns. *Advances in Neural Information Processing Systems*, 32, 2019. 3
- [22] Ziwei Liu, Ping Luo, Shi Qiu, Xiaogang Wang, and Xiaoou Tang. Deepfashion: Powering robust clothes recognition and retrieval with rich annotations. In *Proceedings of the IEEE conference on computer vision and pattern recognition*, pages 1096–1104, 2016. 5
- [23] Ilya Loshchilov and Frank Hutter. Decoupled weight decay regularization. *arXiv preprint arXiv:1711.05101*, 2017. 1
- [24] Zhengyao Lv, Xiaoming Li, Xin Li, Fu Li, Tianwei Lin, Dongliang He, and Wangmeng Zuo. Learning semantic person image generation by region-adaptive normalization. In *Proceedings of the IEEE/CVF Conference on Computer Vision and Pattern Recognition*, pages 10806–10815, 2021. 2
- [25] Yifang Men, Yiming Mao, Yuning Jiang, Wei-Ying Ma, and Zhouhui Lian. Controllable person image synthesis with attribute-decomposed gan. In *Proceedings of the IEEE/CVF conference on computer vision and pattern recognition*, pages 5084–5093, 2020. 2, 5
- [26] Alexander Quinn Nichol and Prafulla Dhariwal. Improved denoising diffusion probabilistic models. In *International*

- Conference on Machine Learning*, pages 8162–8171. PMLR, 2021. 3
- [27] Yurui Ren, Xiaoming Yu, Junming Chen, Thomas H Li, and Ge Li. Deep image spatial transformation for person image generation. In *Proceedings of the IEEE/CVF Conference on Computer Vision and Pattern Recognition*, pages 7690–7699, 2020. 1, 2, 5, 6, 8
- [28] Yurui Ren, Yubo Wu, Thomas H Li, Shan Liu, and Ge Li. Combining attention with flow for person image synthesis. In *Proceedings of the 29th ACM International Conference on Multimedia*, pages 3737–3745, 2021. 1
- [29] Yurui Ren, Xiaoqing Fan, Ge Li, Shan Liu, and Thomas H Li. Neural texture extraction and distribution for controllable person image synthesis. In *Proceedings of the IEEE/CVF Conference on Computer Vision and Pattern Recognition*, pages 13535–13544, 2022. 2, 5, 6
- [30] Robin Rombach, Andreas Blattmann, Dominik Lorenz, Patrick Esser, and Björn Ommer. High-resolution image synthesis with latent diffusion models. In *Proceedings of the IEEE/CVF Conference on Computer Vision and Pattern Recognition (CVPR)*, pages 10684–10695, 2022. 7
- [31] Ruizhi Shao, Gaochang Wu, Yuemei Zhou, Ying Fu, Lu Fang, and Yebin Liu. Localtrans: A multiscale local transformer network for cross-resolution homography estimation. In *Proceedings of the IEEE/CVF international conference on computer vision*, pages 14890–14899, 2021. 4
- [32] Aliaksandr Siarohin, Enver Sangineto, Stéphane Lathuilière, and Nicu Sebe. Deformable gans for pose-based human image generation. In *Proceedings of the IEEE conference on computer vision and pattern recognition*, pages 3408–3416, 2018. 1, 2, 5
- [33] Jiaming Song, Chenlin Meng, and Stefano Ermon. Denoising diffusion implicit models. *arXiv preprint arXiv:2010.02502*, 2020. 5
- [34] Garvita Tiwari, Dimitrije Antić, Jan Eric Lenssen, Nikolaos Sarafianos, Tony Tung, and Gerard Pons-Moll. Pose-ndf: Modeling human pose manifolds with neural distance fields. In *European Conference on Computer Vision*, pages 572–589. Springer, 2022. 4
- [35] Ashish Vaswani, Noam Shazeer, Niki Parmar, Jakob Uszkoreit, Llion Jones, Aidan N Gomez, Łukasz Kaiser, and Illia Polosukhin. Attention is all you need. *Advances in neural information processing systems*, 30, 2017. 1
- [36] Zhou Wang, Alan C Bovik, Hamid R Sheikh, and Eero P Simoncelli. Image quality assessment: from error visibility to structural similarity. *IEEE transactions on image processing*, 13(4):600–612, 2004. 1
- [37] Thomas Weng, David Held, Franziska Meier, and Mustafa Mukadam. Neural grasp distance fields for robot manipulation. In *2023 IEEE International Conference on Robotics and Automation (ICRA)*, pages 1814–1821. IEEE, 2023. 4
- [38] Haofei Xu, Jing Zhang, Jianfei Cai, Hamid Rezatofighi, and Dacheng Tao. Gmflow: Learning optical flow via global matching. In *Proceedings of the IEEE/CVF conference on computer vision and pattern recognition*, pages 8121–8130, 2022. 4
- [39] Jinsong Zhang, Kun Li, Yu-Kun Lai, and Jingyu Yang. Pise: Person image synthesis and editing with decoupled gan. In *Proceedings of the IEEE/CVF Conference on Computer Vision and Pattern Recognition*, pages 7982–7990, 2021. 2, 5
- [40] Pengze Zhang, Lingxiao Yang, Jian-Huang Lai, and Xiaohua Xie. Exploring dual-task correlation for pose guided person image generation. In *Proceedings of the IEEE/CVF Conference on Computer Vision and Pattern Recognition*, pages 7713–7722, 2022. 5, 8
- [41] Richard Zhang, Phillip Isola, Alexei A Efros, Eli Shechtman, and Oliver Wang. The unreasonable effectiveness of deep features as a perceptual metric. In *Proceedings of the IEEE conference on computer vision and pattern recognition*, pages 586–595, 2018. 1
- [42] Liang Zheng, Liyue Shen, Lu Tian, Shengjin Wang, Jingdong Wang, and Qi Tian. Scalable person re-identification: A benchmark. In *Proceedings of the IEEE international conference on computer vision*, pages 1116–1124, 2015. 5
- [43] Xingran Zhou, Bo Zhang, Ting Zhang, Pan Zhang, Jianmin Bao, Dong Chen, Zhongfei Zhang, and Fang Wen. Cocosnet v2: Full-resolution correspondence learning for image translation. In *Proceedings of the IEEE/CVF Conference on Computer Vision and Pattern Recognition*, pages 11465–11475, 2021. 2, 5
- [44] Xinyue Zhou, Mingyu Yin, Xinyuan Chen, Li Sun, Changxin Gao, and Qingli Li. Cross attention based style distribution for controllable person image synthesis. In *European Conference on Computer Vision*, pages 161–178. Springer, 2022. 2, 5, 6, 7
- [45] Zhen Zhu, Tengting Huang, Baoguang Shi, Miao Yu, Bofei Wang, and Xiang Bai. Progressive pose attention transfer for person image generation. In *Proceedings of the IEEE/CVF Conference on Computer Vision and Pattern Recognition*, pages 2347–2356, 2019. 1, 5, 7, 8

RePoseDM: Recurrent Pose Alignment and Gradient Guidance for Pose Guided Image Synthesis

Supplementary Material

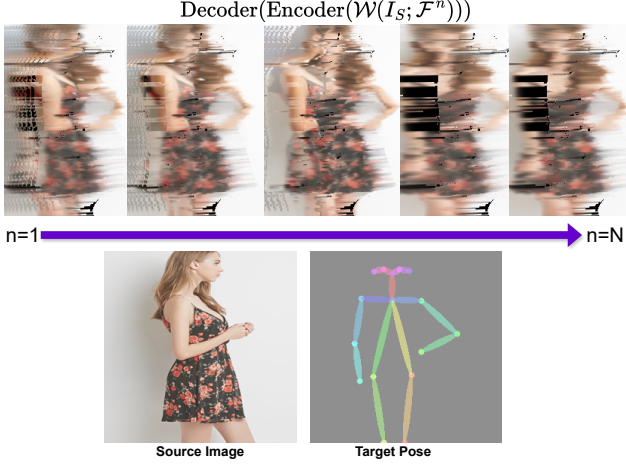


Figure 8. VAE Decoder Output of Recurrent Pose Alignment (RPA) for N iterations, depicting the ability to transfer pose as well as texture

6. Motivation

The figure 8 depicts the functioning of the CNN-based Recurrent Pose Alignment. Clearly, the decoded and warped RGB image contains the target pose while retaining the textures of the input image (red color flowers). However, it still contains minor traces of the pose from the input image. We can see the effectiveness of Recurrent Pose Alignment from the decoded output which filters out the source pose as the iterations approaches N . This is due to multi-level warping applied on the source image after recurrent accumulation. The U-Net of the diffusion model is trained solely using the mean squared error between the initial noise and the predicted noise, given as:

$$L_{mse} = \mathbb{E}_{t \sim [0, T], y_0 \sim q(y_0), \epsilon} \|\epsilon - \tilde{\epsilon}_\theta(y_t, t, P, I_S)\|^2 \quad (18)$$

Since the above equation for predicted error is in no way related to the pose leakage error, hence the predicted image with source pose error is shown in Figure 5 with Baseline B2. Due to this, we have added the error related to pose generated at each time step and guide the U-Net towards the actual pose. We called the poses generated at each time step the interaction poses. Since the valid interaction pose is already known, we derive the error related to the pose as well. If this error is added at each time step the diffusion learns to minimise the pose error as well. We update the sample generated at each time step with the gradient of the

pose error to drive the changes in the direction of maximum pose error with respect to the target pose. This is depicted in the paper with the equation given as:

$$y'_{t-1} = y_{t-1} - \underbrace{\nabla_{\tilde{P}_t} G_\phi(\tilde{P}_t)}_{\Delta y_{0,t}} \quad (19)$$

Hence, the combined effect of Recurrent Pose Alignment and Gradient Guidance prove the effectiveness in pose guided image generation.

7. Evaluation Metrics

Model performance is evaluated using three different evaluation metrics: Structural Similarity Index Measure (SSIM) [36], Learned Perceptual Image Patch Similarity (LPIPS) [41], and Fréchet Inception Distance (FID) [13]. Collectively, SSIM and LPIPS are used to capture reconstruction accuracy. SSIM calculates pixel-level image similarity, while LPIPS computes the perceptual distance between the generated images and reference images by employing a network trained on human judgments. FID calculates the Wasserstein-2 distance between distributions of the generated images and the ground-truth images, it quantifies the realism of the generated images.

8. Implementation Details

All experiments were carried out on 8 NVIDIA A100 GPUs. We trained our diffusion model for 300K iterations with a batch size of 8 using the AdamW optimizer [23] with a learning rate of 10^{-4} . For training with unconditional guidance, we set $p = 10$. We used $T = 1000$ diffusion steps with a linear noise schedule. The diffusion step t was sampled from a uniform distribution at each training iteration. Moreover, during training, we adopted an exponential moving average (EMA) of denoising network weights with a decay rate of 0.9999. For RPA, we use $N=5$. For sampling, the value of conditional guidance was set to $w_c = 2$. For the DeepFashion dataset, we trained our model using 256×176 and 512×352 images. For Market-1501, we used 128×64 images.

9. High Resolution Results

We provide the high resolution results for pose guided image synthesis is shown in Figure 9 and 10.



Figure 9. Qualitative comparison of several SOTA methods on the DeepFashion dataset. The inputs shown are target pose and source image, ground truth shows the image in target pose. Images generated from several methods are shown next. Ours indicate RePoseDM



Figure 10. Qualitative comparison of several SOTA methods on the DeepFashion dataset. The inputs shown are target pose and source image, ground truth shows the image in target pose. Images generated from several methods are shown next. Ours indicate RePoseDM